coatings

MDPI

Article

The Effect of Direct and Pulsed Current in the Presence of Surfactants on the Electrodeposition of Zn–SiC Nanocomposite Coatings

Honorata Kazimierczak [1,2,*], Krzysztof Szymkiewicz [2], Eliezer Gileadi [3] and Noam Eliaz [1]

[1] Biomaterials & Corrosion Laboratory, Department of Materials Science and Engineering, Tel-Aviv University, Ramat Aviv 6997801, Israel; neliaz@tau.ac.il
[2] Institute of Metallurgy and Material Science, Polish Academy of Sciences, Reymonta 25, 30-059 Krakow, Poland; k.szymkiewicz@imim.pl
[3] School of Chemistry, Faculty of Exact Sciences, Tel-Aviv University, Ramat Aviv 6997801, Israel; gileadi@post.tau.ac.il
* Correspondence: honorata.kazimierczak@gmail.com; Tel.: +972-3-640-6201

Received: 30 December 2018; Accepted: 31 January 2019; Published: 3 February 2019

Abstract: Zn–SiC nanocomposite coatings were electrodeposited from aqueous citrate electrolytes using either direct current deposition (DCD) or pulsed electrodeposition (PED). The effects of various surface-active organic compounds (SDS, gum arabic, gelatin, CTAB, PEG 20000, and Triton X–100) on the coatings' surface morphology and chemical composition were studied. The influence of pulse frequency and duty cycle on the percentage of the SiC nanoparticles (NPs) incorporated and on the quality of the deposits was also investigated. The amount of SiC NPs incorporated in the Zn matrix was similar for layers obtained by DCD compared to PED. The Zn–SiC coating deposited by PED exhibited a more fine-grained surface morphology. The percentage of SiC co-deposited with Zn was mainly affected by the type of surfactant used. The ionic surfactants (cationic gelatin and CTAB or anionic gum arabic) allowed the co-deposition of considerably higher amounts of SiC NPs with Zn, compared to the non-ionic compounds PEG 20000 and Triton X–100. However, the use of high molecular weight organic compounds such as gelatin and gum arabic led to aggregation of SiC NPs within the Zn matrix.

Keywords: nanocomposite coatings; silicon carbide; zinc; pulsed current electrodeposition; surfactants

1. Introduction

Zinc is a vital metal from technological and industrial perspectives, due to its key role as a component of protective coatings. The incorporation of ceramic particles into the zinc matrix can be considered as an effective way to improve its mechanical and corrosion properties. The incorporation of second phase micro- or nano-particles (NPs) into a metal matrix may result in the substantial improvement of a variety of properties of the composite material (such as microhardness, yield strength, tensile strength, wear and corrosion resistance, self-lubrication, high-temperature inertness, and chemical and biological compatibility) in comparison with the characteristics of a pure metal or alloy, hence it remains the subject of much research [1–4].

Electrodeposition offers a versatile way to produce high-quality composite coatings with well-dispersed NPs, a smooth surface, and a good coating/substrate bonding, in a single step, at low cost, and using an easily controllable and reproducible procedure. Moreover, it can ensure continuous processing and the capability to handle complex geometries or non-line-of-sight surfaces [1,5,6].

Silicon carbide (SiC) micro- and nano-particles are of considerable interest as the reinforcing phase [3,4,7,8]. The matrix phase studied so far has been mainly Ni and its alloys [3,9–14], whereas much less has been reported on SiC co-electrodeposition with Zn [15–18].

Pulse plating has widely been used to increase the uniformity, adhesion, and speed of electrodeposition [1,19–25]. Pulse plating also allows enhancement of the incorporation of inert particles in the deposit [22], affects the nucleation centers [24], and leads to grain refinement and to a better compactness of the deposit [23].

Roventi et al. [26,27] formed Zn–SiC via pulsed electrodeposition (PED) from a slightly acidic chloride bath. In the first attempt [26], a very low amount of SiC was incorporated (<0.1 wt.%); hence, in the next step [27] gelatin was added to the bath, leading to the formation of uniform coatings containing from 1.7 wt.% to 2.1 wt.% SiC. Sajjadnejad et al. [4,28] investigated the formation of Zn–SiC nanocomposite coatings by both direct current deposition (DCD) and PED from a borate bath at pH = 4.5. Sodium dodecyl sulphate (SDS) was added to the bath to decrease the hydrophobicity and influence the charge stabilization of the suspension. In the case of DCD, the maximum concentration of embedded SiC NPs was only 0.96 vol.% (0.43 wt.%). The application of PED resulted in significant increase of the SiC incorporation, up to 10 vol.% (4.76 wt.%) at a duty cycle of 0.5 and pulse frequency of 100 Hz, with a maximum applied current density of 12 A·dm^{-2}.

The modification of the surface morphology and composition of electrodeposited composites can also be achieved by the use of surface-active compounds [1,25]. Such additives, which are often organic compounds, can adsorb to the substrate, to the suspended inert particles, or to the growing deposit, thus influencing the electrodeposition process and deposit properties. Moreover, the presence of proper organic additives facilitates the suspension of inert particles, prevents particle aggregation, and increases the composite's particle content [29]. The chemical structures of several additives that are further discussed and investigated are presented in Figure 1.

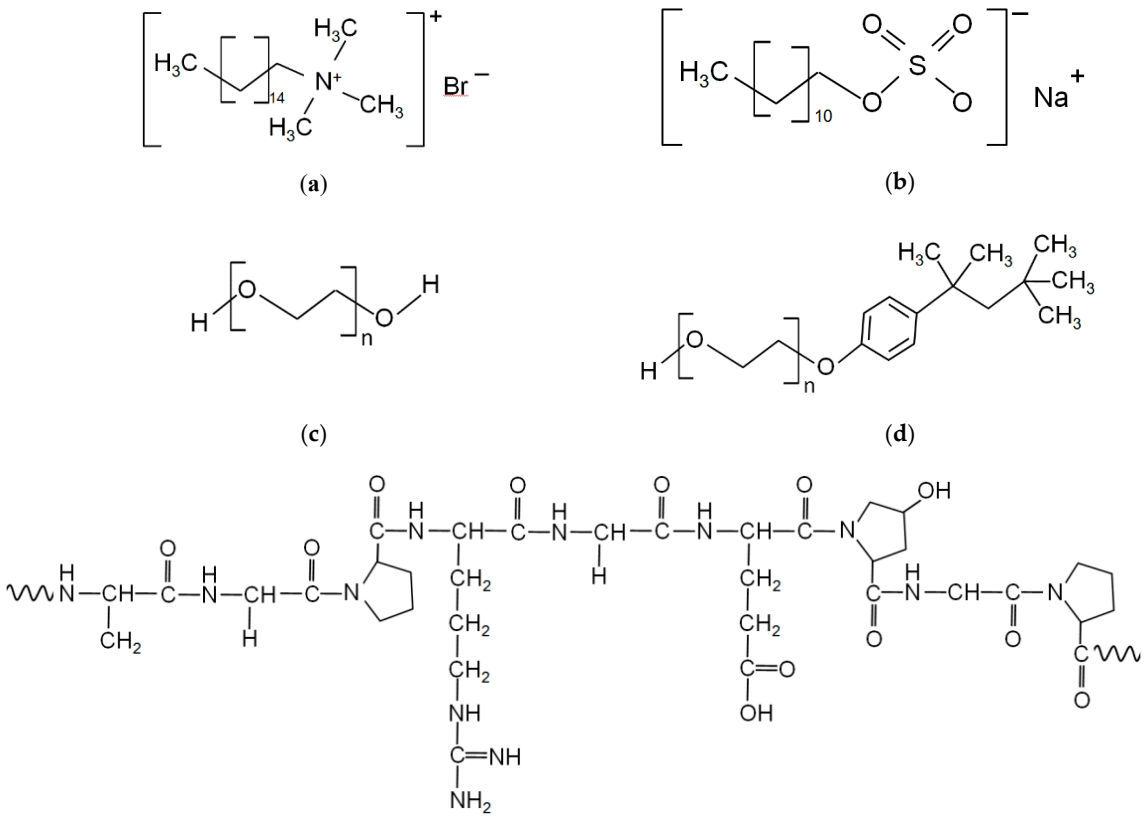

Figure 1. *Cont.*

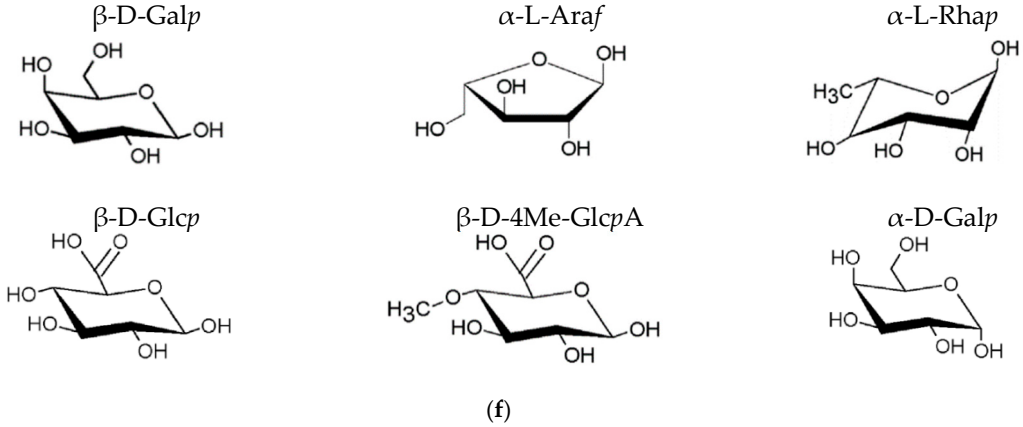

Figure 1. The chemical structures of the organic additives investigated: (**a**) Cetyl trimethyl ammonium bromide (CTAB), (**b**) dodecyl sulphate sodium salt (SDS), (**c**) polyethylene glycol (PEG), (**d**) polyethylene glycol tert-octylphenyl ether (Triton X–100), (**e**) gelatin, (**f**) main monosaccharides present in gum arabic. Figure 1f is reproduced with permission from [30]. Copyright 2015 Elsevier.

Organic molecules such as animal-derived glues, gelatin, and gums are widely used in the industry [28,29]. They act in zinc electrodeposition mainly as dendrite inhibitors, grain refiners, and brighteners [31,32]. Gelatin (G) and gum arabic (GA) have also been widely used as dispersants, namely, to avoid the agglomeration of inert particles in aqueous solutions [27,33–35].

Gelatin is a hydrolyzed form of collagen, which is sometimes added to electroplating baths (including for zinc electrodeposition) to control the deposition rate, crystallization, leveling, and brightness of the deposit [36–40]. Gelatin can be defined as an amphoteric surfactant due to the presence of both carboxylic and amino groups. It is a high molecular mass polypeptide (up to 4×10^5 g·mol^{-1}), consisting of 18 non-uniformly-distributed amino acid chains with both positive and negative charges (Figure 1e) [41]. Gelatin exhibits cationic behavior at pH values below its isoelectric point (pH < 6–9 for gelatin A, pH < 4.7–5.4 for gelatin B) due to the protonation of amino groups [41,42].

Gum arabic is an anionic surfactant. It is a complex and highly branched polysaccharide, which consists of neutral (Gal, Ara, and Rha) and acidic (GlcA and 4Me-GlcA) monosaccharides and protein fractions (Figure 1f) [30]. The molecular weight of GA varies between 2.5×10^5 and 1×10^6 g·mol^{-1}. Due to the presence of carboxyl groups, it is negatively charged at pH values above 2.2, while at lower pH values the dissociation of the carboxyl groups is suppressed [30,43,44].

In recent years, polyethylene glycol (PEG) polymers of different molecular weights (4×10^2 to 2×10^4 g·mol^{-1}) have been studied extensively as surface-active agents in the process of electrodeposition of alloys, and its role in the electrodeposition process has been widely analyzed [45–47]. It has been found that the presence of PEG in an electrolyte results in the formation of homogeneous, smooth, and compact metallic coatings [48,49].

Polyethylene glycol tert-octylphenyl ether (also known as Triton X–100) has been observed to act as an effective dispersing agent and as an additive controlling surface morphology in the Zn electrodeposition process [50]. Neither Triton X–100 nor PEG 20000 molecules have charged groups, hence they are examples of non-ionic polymeric surfactants (Figure 1c,d).

Another interesting surfactant applied to improve the dispersion and incorporation of second-phase NPs into a metal matrix is cetyl trimethyl ammonium bromide (CTAB) (Figure 1a). Kumar et al. [7] reported the Zn–SiC nanocomposite formation by DC electrodeposition from a sulphate-borate plating bath containing suspended SiC NPs and CTAB as a surfactant. The selected bath and process parameters led to the formation of a Zn-based composite containing up to 0.48 wt.% of SiC. CTAB is an amine-based cationic surfactant recognized as having strong capability for adsorption on NPs [51]. It is widely used as a stabilizer and structure-directing agent controlling nucleation and the growth of crystallites [3,7,14].

Sodium dodecyl sulphate (SDS), Figure 1b, is by far the most widely used anionic surfactant. The addition of SDS to the plating bath may result in the formation of uniform zinc deposits [50,52]. It has also been utilized as a colloid stabilizer and as a dispersant [14,28,35].

Previously we investigated, for the first time, the DC co-deposition of Zn–SiC from aqueous citrate bath with gelatin as a bath additive [53,54]. The optimal parameters of the zinc-citrate bath were chosen on the basis of the analysis of a thermodynamic model. The effect of the applied current density, bath composition, and hydrodynamic conditions were studied [53]. Zeta potential measurements confirmed the adsorption of citrate and citrate-zinc ions as well as gelatin molecules on the surface of the SiC NPs. It was shown that SiC co-deposition with Zn proceeds through the entrapment of ceramic NPs during the reduction of citrate-zinc ions firstly adsorbed on their surface as well as by the mechanical entrapment of NPs agglomerates in the cavities formed in the Zn deposit [53,54].

The work presented herein aimed to investigate if the composition and morphology of Zn–SiC composites deposited from aqueous citrate baths can be further modified and optimized by the application of PED and the use of different surfactants. The combined effect of DCD and PED, along with various organic additives, such as cationic CTAB, anionic SDS, and gum arabic, non-ionic PEG 20,000 and Triton X–100, as well as amphoteric gelatin, on the process of Zn–SiC co-deposition is studied. The influence of the different nature of these surfactants and electrodeposition parameters on the NPs content and distribution within Zn matrix is discussed too.

2. Materials and Methods

The electrolyte solutions were prepared by dissolving 0.25 M of sodium citrate and 0.20 M of zinc sulphate in deionized water (18.2 $M \cdot cm^{-1}$), followed by the addition of 80 $g \cdot dm^{-3}$ SiC NPs. Each organic additive was added to the bath in the following concentration: 1 $g \cdot dm^{-3}$ CTAB (Sigma-Aldrich, St. Louis, Missouri, USA), 0.1 $g \cdot dm^{-3}$ SDS (Sigma-Aldrich), 1 $g \cdot dm^{-3}$ gum arabic (Chempur, Piekary Śląskie, Poland), 1 $g \cdot dm^{-3}$ PEG 20000 (Sigma-Aldrich), 0.2 $g \cdot dm^{-3}$ Triton X–100 (Sigma-Aldrich), and 1 $g \cdot dm^{-3}$ gelatin (Chempur). The solution pH was adjusted to 4.5 by the addition of sulphuric acid. All chemicals were of analytical grade. Spherical β-SiC NPs supplied by Alpha Aesar (Headfair, MA, USA) were used. The solution obtained in this way was then stirred magnetically for 24 h prior to electrodeposition. The magnetic stirring was maintained at a speed of 200 rpm during the electrochemical experiments.

All electrochemical measurements were carried out in a 200 cm^3 cell at room temperature (~20 °C) in a system with a rotating disc electrode (RDE) [1] to ensure constant and controlled hydrodynamic conditions (ω = 30 $rad \cdot s^{-1}$). The working electrode was a copper disc placed in a sealed Teflon holder (active surface area 2.83 cm^2). A platinum sheet (surface area ~3.5 cm^2) was used as the counter electrode. The working electrode potentials were referred to the saturated calomel electrode (SCE). Copper electrodes were chemically polished using a mixture of concentrated nitric, acetic, and phosphoric acids (1:1:1) at ambient temperature for ca. 10 s. The PED and DCD processes were performed using a ParSTAT 2273 potentiostat (Ametek, Berwyn, PA, USA). Cyclic voltammetry measurements were performed using PGSTAT302N potentiostat (Metrohm Autolab, Utrecht, The Netherlands).

The PED process can be described by the following parameters [1,20,28]: On-time (t_{on}), off-time (t_{off}) peak current density (j_p), and average current density (j_{avg}), where the average current is given by:

$$j_{avg} = j_p \times \theta \quad (1)$$

and the duty cycle θ is defined as:

$$\theta = \frac{t_{on}}{t_{on} + t_{off}} \quad (2)$$

The composition of deposits (Zn and Si) was determined by wavelength dispersive X-ray fluorescence (WDXRF). Analysis was carried out using a Rigaku Primini spectrofluorimeter (Rigaku,

Tokyo, Japan) with scintillation counters (LiF crystal). The weight percentage of SiC in the Zn–SiC composite was calculated from the Zn and Si weight percentages, as described elsewhere [27,53,54], assuming that all Si atoms are bound to C as SiC in a 1:1 molar ratio. The faradaic efficiency (FE) of the process was calculated, as described elsewhere [53,54], assuming that only zinc ions could be deposited on the cathode. The samples were weighed before and after the deposition process using Kern ALT analytical scales with readability of 0.01 mg. The reproducibility of the electrodeposition process was verified using three to five replicates; typical results are reported herein.

The surface morphology and the cross-section of the Zn–SiC composite coatings were characterized by a FEI model Quanta™ 3D field-emission gun (FEG) scanning electron microscope (SEM) (Thermo Fisher Scientific, Hillsboro, OR, USA), equipped with an energy-dispersive X-ray spectroscopy (EDS) Trident system (Apollo 40 EDS spectrometer, EDAX Inc., Mahwah, NJ, USA).

SiC nanopowders were imaged in their as-received condition in a Tecnai G2 F20 transmission electron microscope (TEM) (Thermo Fisher Scientific, Hillsboro, OR, USA). The powders were first placed on a copper grid supported by a thin carbon layer. Quantitative analysis of the size distribution of SiC NPs was conducted on TEM images using an ImageJ open source image processing program (https://imagej.net/Welcome).

3. Results and Discussion

Aqueous citrate solutions were proposed as baths for electrodeposition of Zn–SiC composite coatings due to the fact that citrates are non-toxic and form strong complexes with Zn(II). Citrates also provide the stabilization of the pH of electrolyte solutions, hence they are widely used in the electrodeposition of zinc and its alloys [55,56]. The electrolyte composition in this work was selected based on earlier studies of the electrodeposition of zinc-based alloys from aqueous citrate solutions [53,54,56–59]. The only variable in the bath chemistry was the type of organic additive (Figure 1). The Zn–cit electrolyte without SiC NPs and the Zn–cit–SiC solution without any organic additives were used as reference systems in all investigations. The TEM image and electron diffraction pattern of the β-SiC NPs used in this study are shown in Figure 2. It is evident that the NPs are spheres of non-uniform size, ranging from 11 to 390 nm (average of 90 nm).

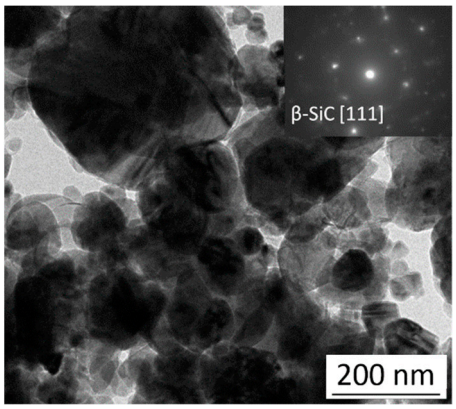

Figure 2. TEM image of spherical β-SiC nanoparticles with diameters ranging from 11 to 390 nm (average of 90 nm).

3.1. Voltammetric Studies

Cyclic voltammetry (CV) measurements were performed in the Zn–cit and Zn–cit–SiC systems with various organic additives (Figures 3 and 4) in order to first estimate the possibility of Zn electrodeposition in the presence of our chosen surfactants and SiC NPs. In all cases considered, a slight rise of cathodic current is observed starting from about −0.85 V, and a limiting current is observed (Figure 3a, inset I; Figure 3b, inset) within a relatively narrow current range, which represents hydrogen evolution from citrate ions H_3Cit^- and H_2Cit^{2-} [53]. Next, when the cathode potential

reaches about −1.15 V, Zn electrodeposition begins (Figures 3 and 4). In the case of Zn–cit bath without any additives (Figures 3a and 4a), a fast increase in cathodic current is observed while shifting the potential towards more negative values. This indicates that an activation-controlled bulk zinc electrodeposition is taking place. Next, during the reverse scan, an anodic peak indicates that the oxidation of previously deposited zinc occurs, starting from a potential of −1.1 V vs. SCE.

The addition of organic additives to the Zn–cit bath (Figure 3a) decreases the cathodic current density in all cases considered, indicating inhibition of Zn electrodeposition. The shape of the CV is analogous to that registered in the Zn–cit bath without additives only in the case of SDS. In contrast, the voltammograms registered in the presence of other organic additives show significant decay of cathodic current density beyond the peak potential at around approximately −1.25 V. This may be attributed to the change of the electrodeposition kinetics—to the mass-transport control under such conditions [60]. Next, as electrode potential is swept to more negative values, the cathodic current density raises again. However, for all cases considered, the cathodic current density values are lower than in the case of additive-free Zn–cit electrolyte. Such suppression of zinc deposition by organic additives is typical and can be explained either by adsorption of surfactant molecules on the cathode surface [53] or by complexation of the metal ions, which makes it more difficult to reduce [61]. However, the surfactants content is several orders of magnitude smaller than the concentration of the zinc ions. Hence, it can be assumed that the surfactants used could not act as a complexing agent in the present study. The significant decrease of the anodic peak intensity confirms the inhibition of Zn electrodeposition in the presence of surfactants compared to surfactant-free Zn–cit bath.

In the Zn–cit–SiC system (Figures 3b and 4), the shape of the voltammetric curves does not change significantly compared to the Zn–cit system, but the registered current density values, both cathodic and anodic, are higher when SiC NPs are added. The most significant increase of the currents is observable only in the case of CTAB and gelatin (Figure 4d,e). This implies that the electrodeposition kinetics is enhanced due to the presence of SiC NPs in the electrolytic bath. The observed kinetic activation of the zinc electrodeposition can be explained by the adsorption of surfactant molecules on the surface of SiC NPs, instead of on the cathode surface, thus limiting its inhibiting effect on the Zn electrodeposition process. In addition, as previously shown [53], cit and Zn–cit ions adsorption on the SiC NPs may change their transport rate to the cathode, thus enhancing the electrodeposition process.

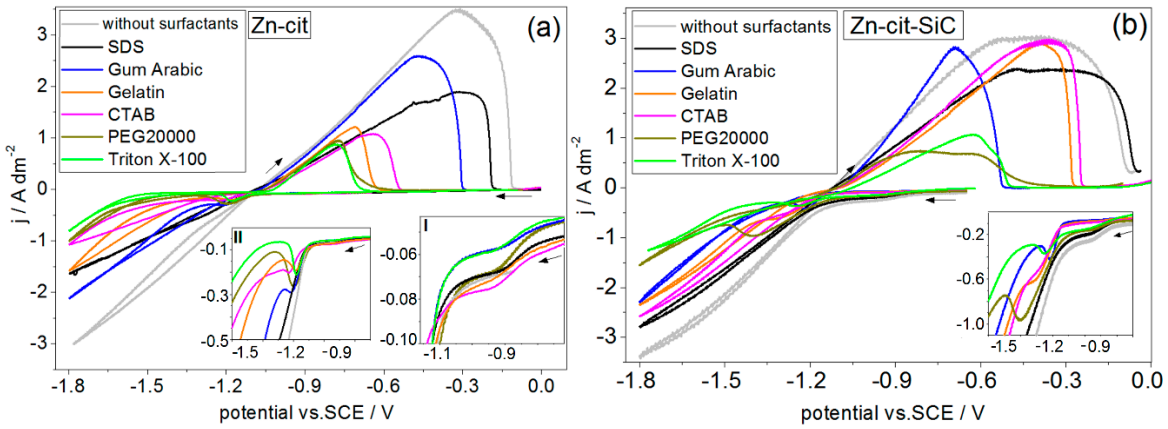

Figure 3. Cyclic voltammograms measured on a Cu substrate in Zn–cit (**a**) and Zn–cit–SiC (**b**) electrolytes with various surfactants added to the bath. ω = 30 rad·s^{-1}, scan rate = 20 mV·s^{-1}, T = 20 °C. Arrows indicate scan direction.

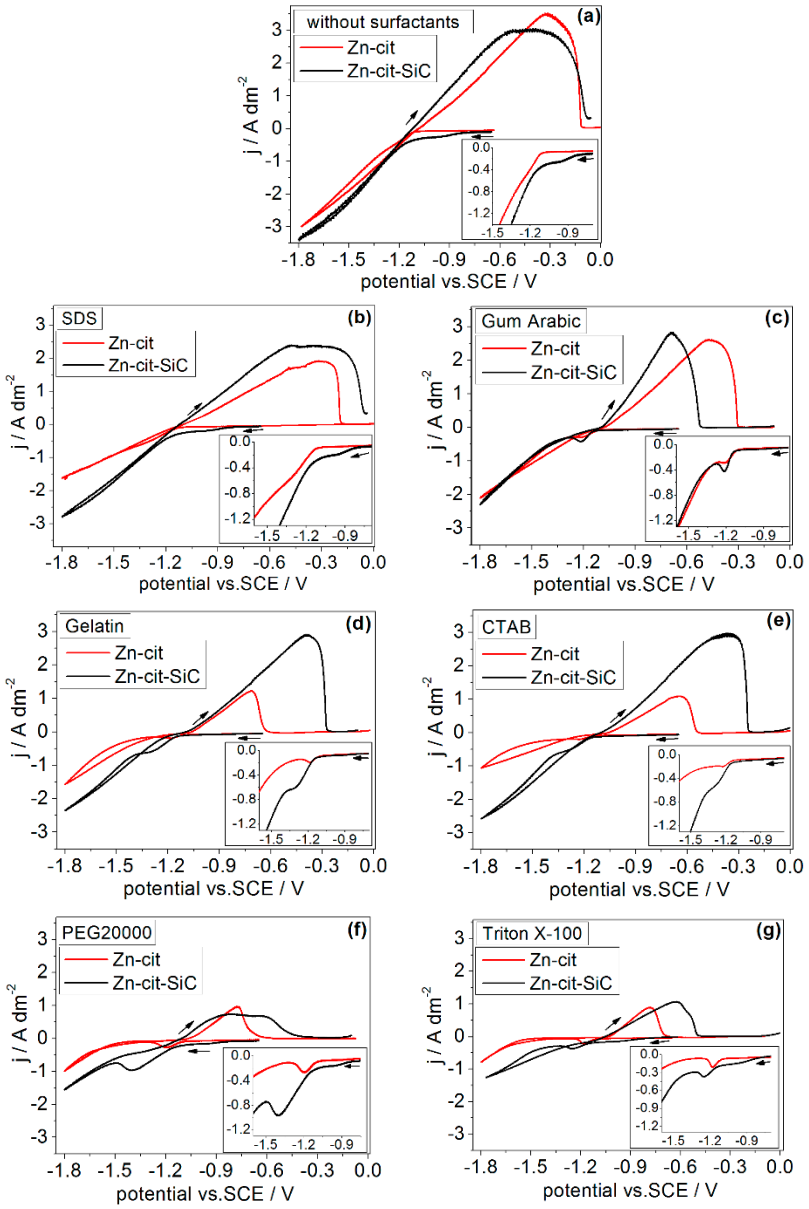

Figure 4. Cyclic voltammograms measured on a Cu substrate in Zn–cit and Zn–cit–SiC electrolytes with or without surfactants: (**a**) Without additives, (**b**) sodium dodecyl sulphate (SDS), (**c**) gum arabic (GA), (**d**) gelatin, (**e**) CTAB, (**f**) PEG, (**g**) Triton X–100. ω = 30 rad·s^{-1}, scan rate = 20 mV·s^{-1}, T = 20 °C. Arrows indicate scan direction.

Summing up, the results of the voltammetric studies indicate that it is possible to deposit zinc from citrate bath in the presence of all studied organic additives and of SiC NPs. The influence of each surfactant on SiC NPs incorporation in the Zn deposit, on the electrodeposition process, and on the quality of the obtained coatings are discussed in the next sections.

3.2. Direct Current Deposition (DCD) from Zn–cit–SiC Baths

DCD is first performed at a pre-selected current density of −3.0 A·dm^{-2}. Figure 5 illustrates the influence of the organic additive used on the SiC content in the composite and on the cathodic current efficiency during plating using direct current. Additionally, it provides the comparison of the results of the DCD process with the exemplary results of the PED process (Figure 5).

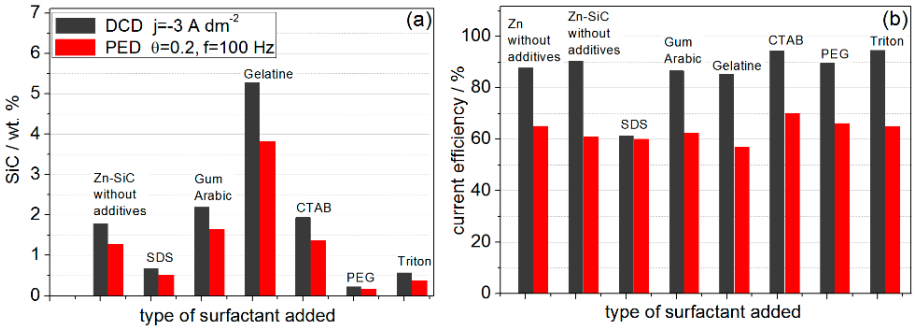

Figure 5. The effect of the type of organic additive on (**a**) the SiC content in Zn–SiC deposit, and (**b**) the faradaic efficiency of the direct current deposition (DCD) process ($j = -3.0$ A·dm^{-2}) compared with result of the PED ($j_{avg} = -3.0$ A·dm^{-2}, $\theta = 0.2$, $f = 100$ Hz).

In the case of DCD the use of the anionic SDS leads to the incorporation of 0.7 wt.% SiC, and the FE is 60%. The addition of anionic GA to the studied solution results in more than a three-fold increase of SiC content in the deposit, compared to that obtained in the presence of SDS (Figure 5a), along with an increase of FE to 90% (Figure 5b). The presence of a cationic surfactant adsorbed on the suspended inert NPs should promote the electrophoretic migration of NPs to the cathode [13]. However, when cationic CTAB is used as a surfactant, the content of the incorporated ceramic NPs and the FE are similar to the results obtained with anionic GA. A marked increase in the weight percentage of SiC is observed with gelatin, which acts as a weak cationic surfactant in the studied system (pH = 4.5). Only in this case is the content of incorporated SiC in the zinc matrix higher than that obtained without surfactants (Figure 5a), and the FE is close to 90% (Figure 5b). With the addition of the non-ionic surfactants PEG 20000 and Triton X–100, the FE is maintained at about 90% (Figure 5b), although the percentage of NPS incorporated decreases to 0.5% (Triton X–100) and 0.3% (PEG 20000) (Figure 5a). Hence, no clear dependence of deposit composition and FE on the nature of surfactant molecules can be stated. Nevertheless, the observed influence of different surfactants on the DCD are analogous to the results of the PED process (Figure 5). This supports the characteristic effect of each surfactant on Zn–SiC deposition from citrate baths. However, the results shown in Figure 5 indicate that both the SiC content and the FE are significantly lower when pulsed current is applied for Zn–SiC deposition. The influence of PED process parameters is discussed in the next sections.

3.3. Pulsed Current Electrodeposition (PED) from Zn–cit–SiC Baths

Next, PED of Zn–SiC layers from baths with various surfactants is studied. Galvanostatic cathodic square waves with an average current density $j_{avg} = -3.0$ A·dm^{-2}, three different frequencies (1, 50, and 100 Hz), and four duty cycle values (0.2, 0.3, 0.4, and 0.5) were applied.

Figure 6 shows the duty cycle dependence of the composition of Zn–SiC layers and the FE of the process. It can easily be seen that the type of organic additive used in the electrolytic bath has the greatest impact on the content of the SiC incorporated in composite layers, and that the tendency is similar to that observed in DCD. The highest content of SiC is present in electrodeposits obtained from the gelatin-containing bath. The addition of anionic GA and cationic CTAB results in SiC content comparable to that obtained in the absence of bath additives. The presence of anionic SDS or non-ionic surfactants such as PEG and Trion results in the decrease of SiC concentration in the deposited composite layers. At a frequency of 1 Hz, the increase of duty cycle values has a noticeable influence only on the co-deposition process in a gelatin-containing bath, namely a distinct increase of SiC content (Figure 6a). At 100 Hz, the SiC content increases along with the increase in duty cycle in GA- and CTAB-containing baths, while the addition of gelatin in this case results in only a very slight increase of SiC content (Figure 6b). For all electrolytes studied, the dependence of the FE on the duty cycle exhibits a similar character (Figure 6b,d). Nevertheless, it is important to note that the incorporation of a relatively high amount of SiC from a gelatin-containing bath is accompanied with a

decrease of FE, compared to the other baths studied. Nevertheless, the addition of any surfactant other than gelatin results in an increase of FE compared to surfactant-free baths; the FE is maintained at a value similar to that in electrodeposition of pure zinc under the same conditions.

Examination of the effect of the applied PED frequency (Figure 7) reveals that the increase of frequency enhances the FE of the process under all conditions (Figure 7b,d,f). The content of SiC increases with frequency, but again, only in cases of gelatin-, GA- and CTAB-containing solutions (Figure 7a,c,e).

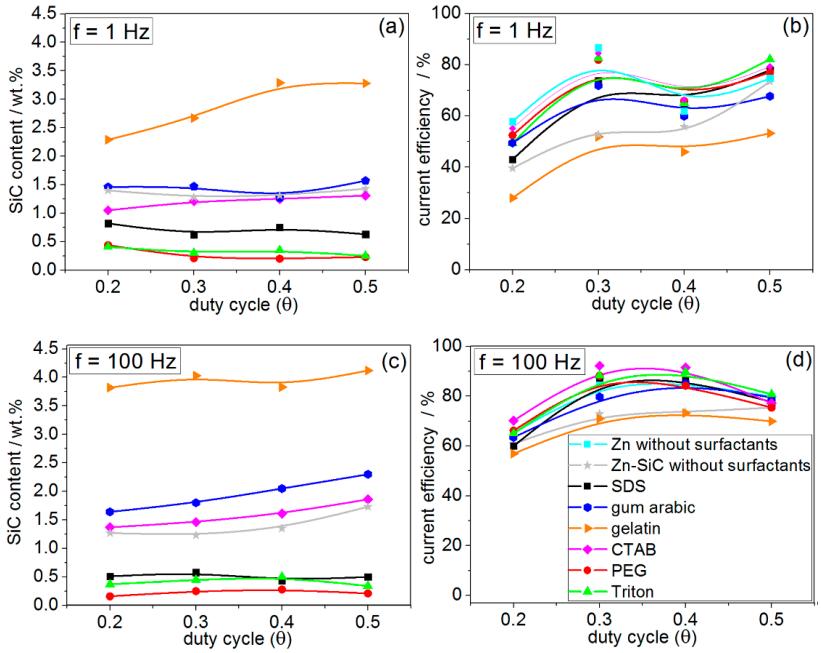

Figure 6. The effect of duty cycle in PED from electrolyte solutions with or without organic on the SiC content in the Zn–SiC deposit (**a**,**c**) and on the faradaic efficiency of the PED process at two selected frequencies–1 Hz (**a**,**b**) and 100 Hz (**c**,**d**).

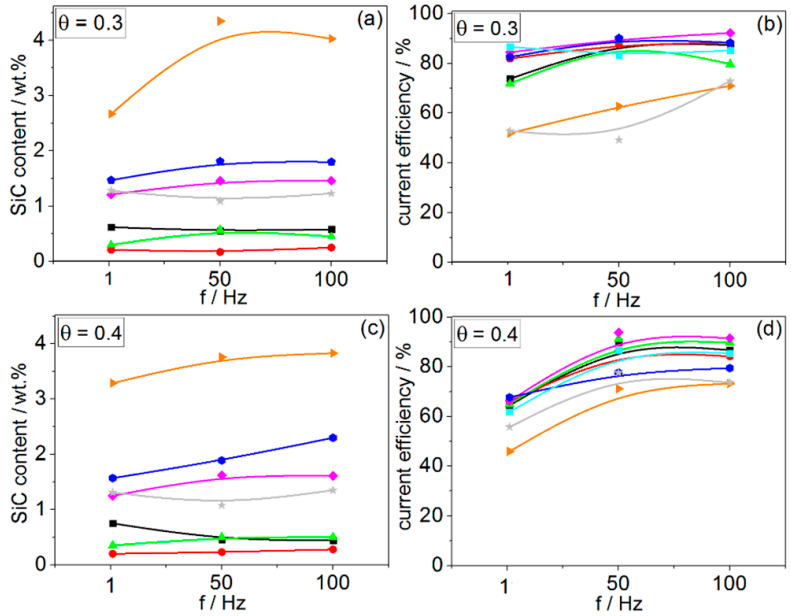

Figure 7. *Cont.*

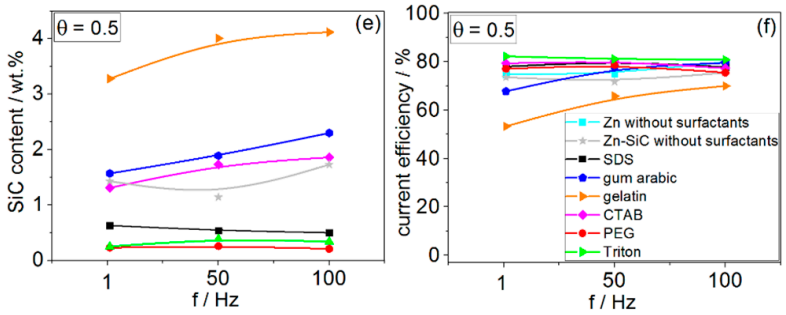

Figure 7. The effect of frequency in PED from electrolyte solutions with or without organic additives on the SiC content in Zn–SiC deposit (**a**,**c**,**e**) and on the faradaic efficiency of the PED process (**b**,**d**,**f**) at different values of duty cycle.

It should be noted that the use of pulsed current substantially hinders the course of the process of Zn–SiC electrodeposition in the absence of surfactants, when compared to DCD; the FE decreases from 93% in the case of DCD to 40%–70% in the case of PED. This is reasonable because during the relaxation time (t_{off}) no deposition takes place, while the enhanced diffusion of ions from the bulk solution to the surface of the cathode does not influence the electrodeposition process since it is activation-controlled in the considered system (Figure 4a). This is consistent with the observation that the FE is the lowest under the lowest duty cycle of 0.2 when the t_{off} is the longest (Figure 6b,d).

3.4. The Surface Morphology of Zn and Zn–SiC Layers

The surface morphologies of Zn and Zn–SiC deposits obtained by DCD are presented in Figure 8a and in Figure 8b–h, respectively. Coatings obtained by DCD without surfactants are not compact, and contain discontinuities that expose the substrate surface underneath (Figure 8a,b). The Zn deposit consists of relatively coarse angular grains (Figure 8a). When SiC is added to the bath without surfactants (Figure 8b), the deposit exhibits a finer and smoother surface (Figure 8b). No agglomerated SiC NPs are visible on the surface in Figure 8b. Addition of the anionic surfactants SDS (Figure 8c) and GA (Figure 8d) results in the formation of a similar morphology comprised of coarser angular grains than in Figure 8b, with some larger protruding semispherical structures. The presence of GA not only results in increased SiC content but also in the formation of a more compact surface compared to that obtained with SDS.

The surface morphologies of Zn–SiC deposits formed in the presence of cationic gelatin and CTAB (Figure 8e,f, respectively) are quite similar. They consist of uniformly distributed grains of similar size, with some pores visible between them. However, the grains formed in the presence of gelatin are more elongated and needle-like, and relatively large agglomerates of SiC are evident on the surface. EDS microanalysis in these pores revealed significantly higher Si content.

The addition of the non-ionic polymeric surfactants PEG 20000 and Triton X–100 (Figure 8g,h, respectively) results in a surface morphology similar to that obtained in the presence of cationic surfactants, but with slightly finer grains. The grains formed in the presence of PEG 20000 are more elongated than those formed with Triton X–100, but in the former case the needle-like shape is associated with lower SiC incorporation. This is opposite to the dependence observed in the case of gelatin versus CTAB. Hence, it can be concluded that the shape of the electrodeposited grains is not related to the amount and distribution of the SiC NPs in the deposit.

The surfaces of deposits obtained by PED are shown in Figures 9–11. The application of PED results in the formation of a finer grain structure, in comparison to DCD. PED improves the quality of pure Zn deposit, which in this case is compact and covers the whole substrate (Figure 9a). PED co-deposition of SiC with Zn, without organic additives, does not change the surface morphology of the composite layer compared to DCD (compare Figure 8b to Figure 9b).

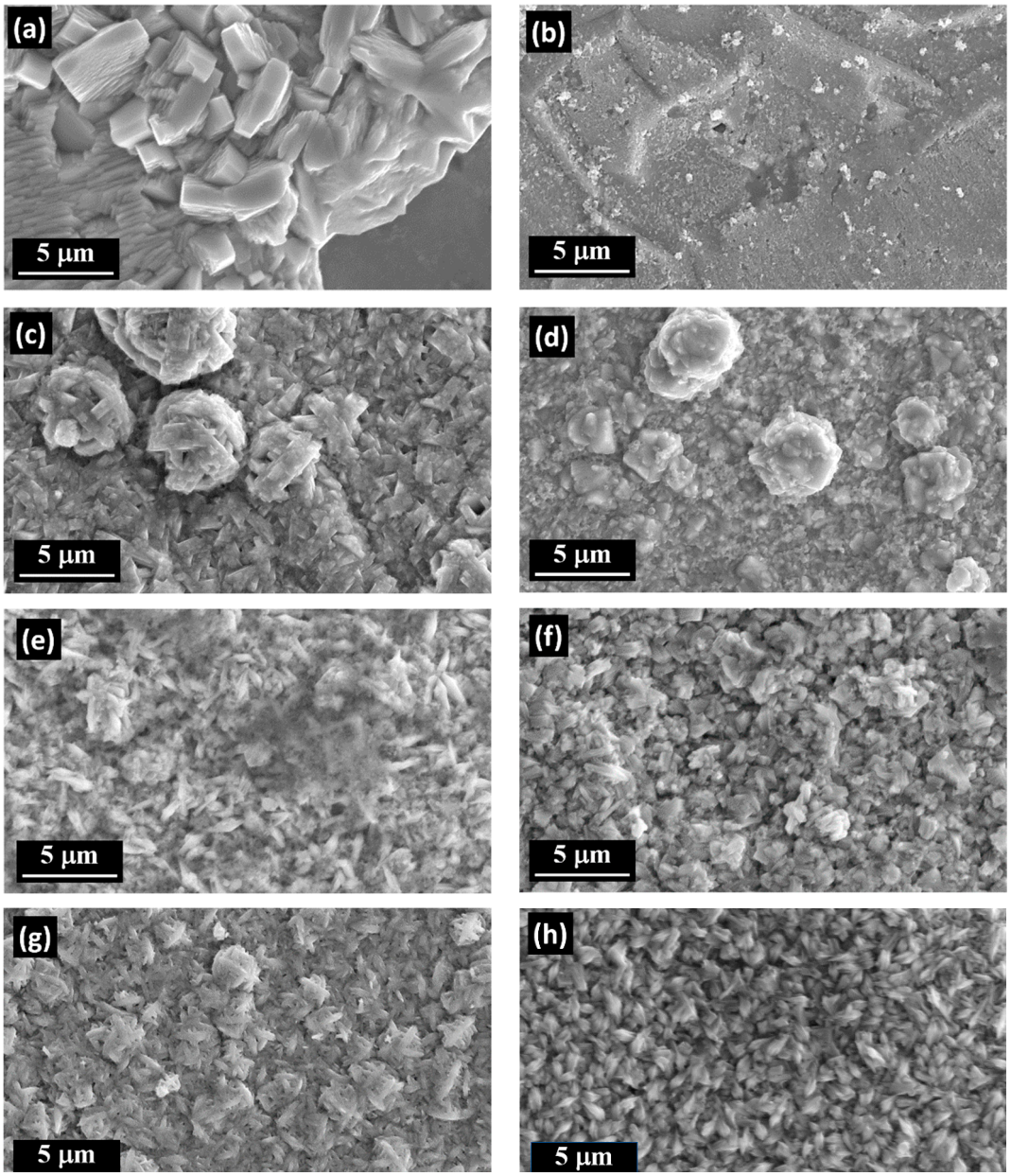

Figure 8. SEM secondary electrons (SE) images of surfaces of Zn (**a**) and Zn–SiC (**b**–**h**) layers formed by DCD at -3.0 A·dm^{-2}, with (**c**–**h**) or without (**a**,**b**) surfactants. (**c**) SDS, (**d**) gum arabic, (**e**) gelatin, (**f**) CTAB, (**g**) PEG 20000, (**h**) Triton X–100.

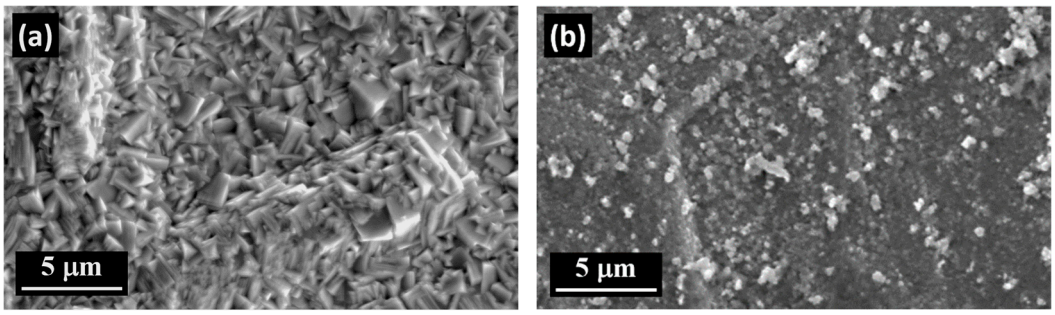

Figure 9. *Cont.*

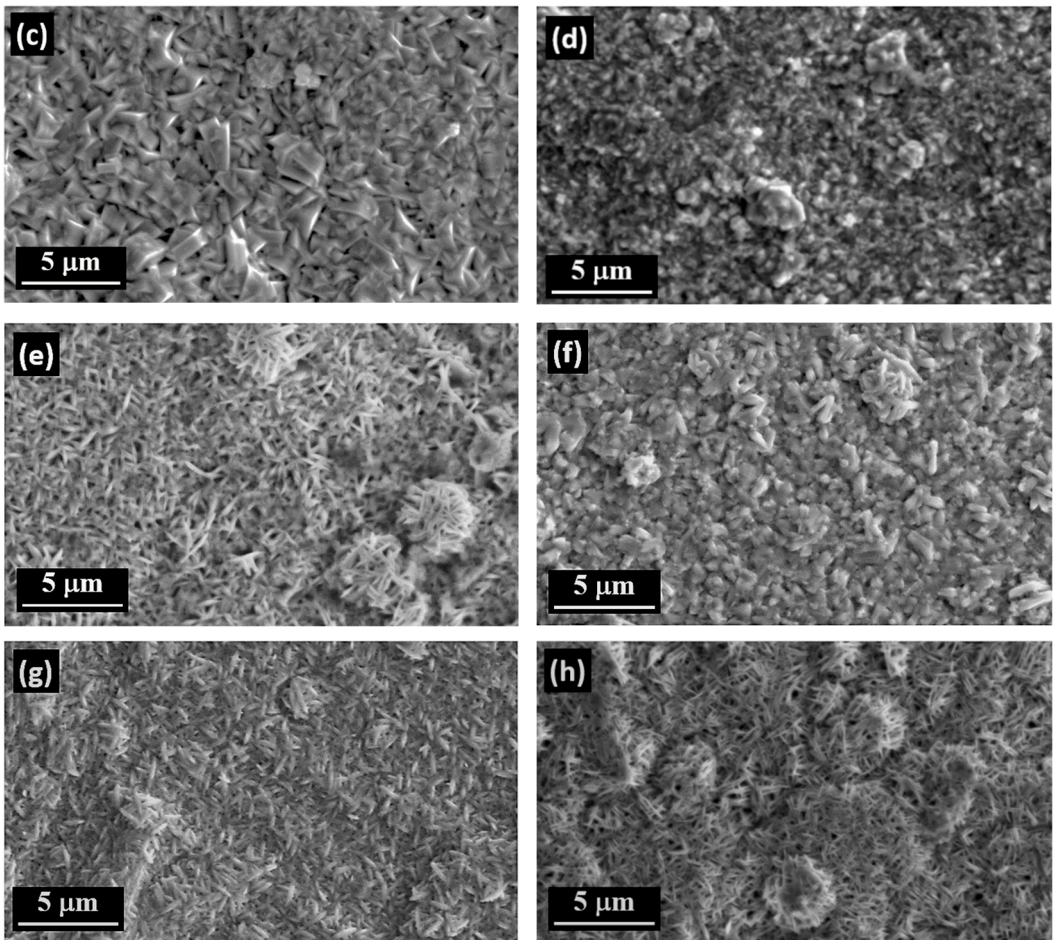

Figure 9. SEM SE images of surfaces of Zn (**a**) and Zn–SiC (**b**–**h**) layers formed by PED at j_{avg} = −3.0 A·dm^{-2}, f = 50 Hz, θ = 0.5, with (**c**–**h**) or without (**a**,**b**) surfactants. (**c**) SDS, (**d**) gum arabic, (**e**) gelatin, (**f**) CTAB, (**g**) PEG 20000, (**h**) Triton X–100.

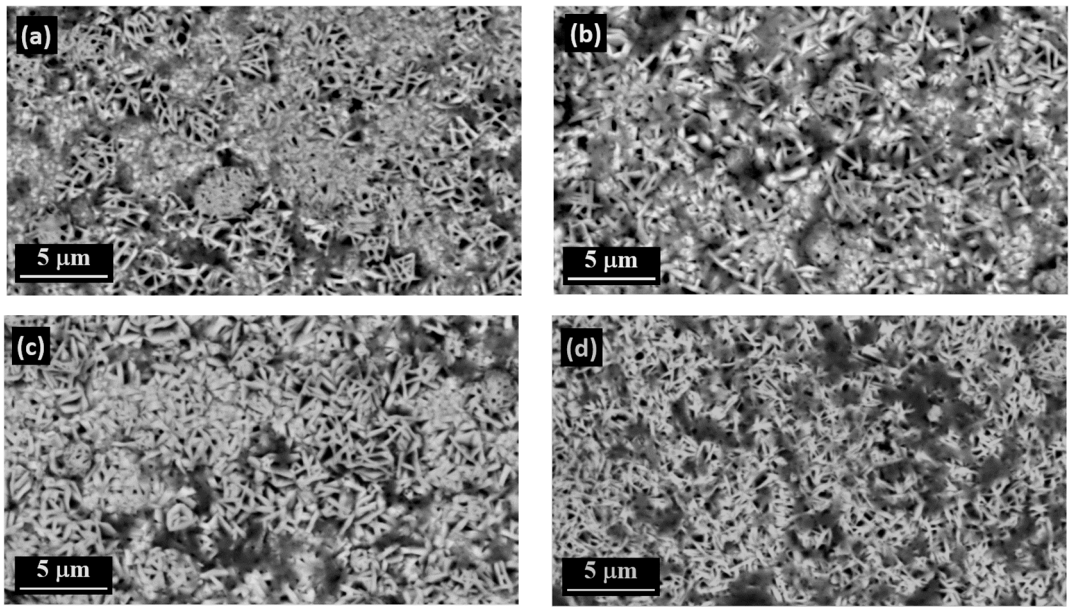

Figure 10. SEM backscatter electrons (BSE) images of the surfaces of Zn–SiC layers formed by PED in the presence of gelatin at j_{avg} = −3.0 A·dm^{-2}, f = 100 Hz, and various values of duty cycle θ: (**a**) 0.2, (**b**) 0.3, (**c**) 0.4, (**d**) 0.5.

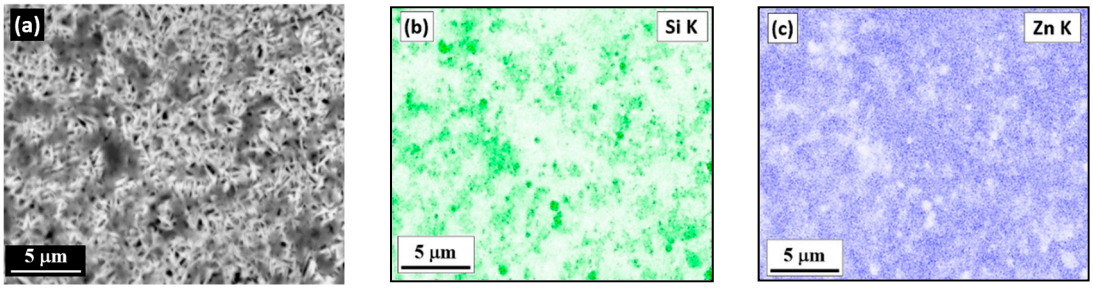

Figure 11. SEM BSE image (**a**) and the corresponding EDS elemental maps of Si (**b**) and Zn (**c**) acquired on the surface of a Zn–SiC layer formed by PED in the presence of gelatin. j_{avg} = −3.0 A·dm^{-2}, f = 100 Hz, and θ = 0.5.

The addition of SDS to the Zn–SiC bath does not change the surface morphology of the PED coating (compare Figure 9c to Figure 9a). The addition of SDS to the Zn–SiC electrolyte allows the incorporation of about 0.5 wt.% of SiC in the Zn matrix. The surface morphology of the PED Zn–SiC(SDS) coating clearly differs from that of the DCD Zn–SiC(SDS) layer, but without the spherical nodules observed in Figure 8c, while the SiC content is similar, i.e., 0.5 wt.%–0.7 wt.%.

The PED Zn–SiC(GA) layers and PED Zn–SiC(CTAB), Figure 9d,f, respectively, have a similar surface morphology. Their surface is relatively smooth and compact. The weight percentage of SiC in the coating is also similar in both cases (1.7 wt.%–1.9 wt.%).

Small SiC agglomerates are also visible on the surface of the PED Zn–SiC(G) layer, see Figures 9e and 11. However, the grains in this case are finer, and the SiC agglomerates are much smaller than those observed in the case of DCD Zn–SiC(G), see Figure 8e. Consequently, the content of SiC decreases from 5.4 wt.% to 4 wt.% for DCD and PED Zn–SiC(G), respectively.

The addition of the non-ionic surfactants PEG 20000 and Triton X–100 (Figure 9g,h, respectively) results in the formation of a needle-like surface morphology by PED. The level of porosity is higher in the case of Triton X–100. The weight percentage of SiC NPs, however, is similar in both cases.

The effect of duty cycle on the surface morphology of PED Zn–SiC(G) is demonstrated in Figures 10 and 11. It is evident that the duty cycle does not affect the surface morphology and the extent of SiC dispersion under these conditions. The concentration of SiC is similar in all four cases and is ~4 wt.%. All four layers are porous, with evidence to SiC agglomerates at the surface. Figure 11b,c shows the EDS Si and Zn elemental maps. Comparison to the SEM BSE image (Figure 11a) reveals the presence and typical size of the SiC NPs. It is confirmed that the dark grey spots visible on the surface are indeed agglomerates of SiC NPs.

Finally, the cross-sections of Zn–SiC coatings were analyzed by SEM. Figure 12 shows the BSE SEM images of selected DCD and PED Zn–SiC coatings with relatively high amounts of SiC NPs, with and without surfactants. Dark spots in these SEM images represent SiC NPs, while the Zn matrix appears white. The distribution of NPs is similar in layers formed by DCD and PED. Differences in the microstructure result only from the type of surfactant added to the plating bath. In all cases, the SiC NPs are embedded as agglomerates. However, with GA the SiC NPs are the smallest, and the content of SiC is about 2 wt.%. The addition of gelatin results in the largest SiC agglomerates, with high amounts of relatively small particles distributed between them. The cross-sections of Zn–SiC(CTAB) and Zn–SiC(G) are similar, except that noticeably less SiC NPs are incorporated in the former. When no bath additives are used, the distribution of SiC NPs is less uniform, namely there are agglomerates along with larger areas of pure Zn (Figure 12a,b).

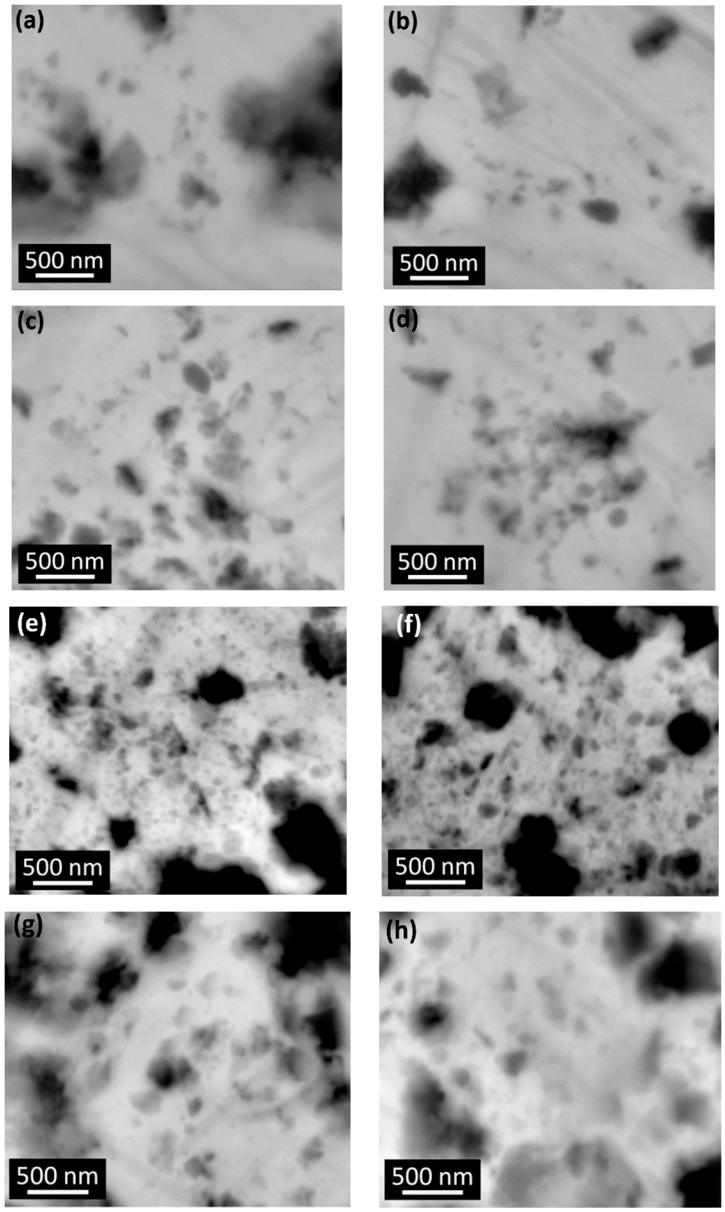

Figure 12. SEM BSE images of the cross-sections of selected Zn–SiC layers formed by either DCD (**a**,**c**,**e**,**g**) or PED (**b**,**d**,**f**,**h**), with (**c**–**h**) or without (**a**,**b**) organic bath additives. (**a**) 1.8 wt.% SiC, FE = 93.1%, (**b**) 1.1 wt.% SiC, FE = 71.6%, (**c**) gum arabic, 2.2 wt.% SiC, FE = 86.6%, (**d**) gum arabic, 1.9 wt.% SiC, FE = 77.6%), (**e**) gelatin, 5.4 wt.% SiC, FE = 85.3%, (**f**) gelatin, 4.0 wt.% SiC, FE = 65.7%, (**g**) CTAB, 1.9 wt.% SiC, FE = 94.5%, (**h**) CTAB, 1.7 wt.% SiC, FE = 80.2%. All PED experiments were carried out at $j_{avg} = -3.0$ A·dm^{-2}, $f = 50$ Hz, $\theta = 0.5$.

4. Conclusions

Zn–SiC composite coatings were successfully synthesized from non-toxic citrate aqueous baths using either direct current deposition (DCD) or pulsed electrodeposition (PED). It is concluded that:

- The amount of SiC NPs incorporated in the Zn matrix is similar in both DCD and PED layers. In both cases NPs are distributed throughout the bulk of the coatings in the form of agglomerates of different sizes.
- The main advantage of PED compared to DCD is the formation of Zn–SiC layers with finer surface morphology.

- The most significant modification of both surface morphology and SiC distribution is accomplished through the use of different types of surface-active organic compounds. The weight percentage of SiC co-deposited with Zn is also mainly affected by the type of surfactant used.
- No significant effect of PED on the SiC incorporation in the Zn matrix can be explained by activation-controlled Zn electrodeposition and SiC incorporation via the reduction of Zn–cit ions adsorbed on the SiC NPs under the studied range of process parameters. Under such conditions, during the relaxation time (t_{off}) no deposition takes place, while the enhanced diffusion of ions from the bulk solution to the cathode surface does not influence either the Zn electrodeposition processes or SiC incorporation.
- The comparison of cyclic voltammograms obtained in cit-Zn and ci-Zn-SiC systems with various surfactants, indicate that surfactant molecules adsorb on the surface of SiC NPs, thus limiting its inhibiting effect on the Zn electrodeposition process.
- Ionic surfactants allow co-deposition of higher amounts of SiC NPs compared to non-ionic surfactants. Electrostatic forces may play a significant role in the incorporation of SiC NPs in the Zn matrix during electrodeposition from citrate baths.
- The Zn–SiC layers obtained in the presence of cationic gelatin as well as anionic gum arabic show considerable SiC NP aggregation. A common feature of these two oppositely charged surfactants is that both are characterized by high molecular weight and a highly branched structure of molecules. Hence, the size and structure of these macromolecules may affect the agglomeration of the ceramic NPs, which then results in a higher than average content of SiC incorporated in the Zn. On the other hand, the use of cationic CTAB (with significantly lower molecular weight and relatively simpler molecular structure) results in the formation of more compact surfaces, with relatively well-dispersed SiC NPs.

Author Contributions: Conceptualization, H.K.; data curation, K.S.; formal analysis, H.K.; investigation, H.K. and K.S.; supervision, E.G. and N.E.; writing—original draft, H.K. and N.E., writing—review and editing, N.E. and H.K.

Funding: The research was initiated and mainly conducted within the framework of project No. LIDER/007/151/L-5/13/NCBR/2014 financed by the National Centre for Research and Development in Poland. The cooperation between the Institute of Metallurgy and Materials Science of the Polish Academy of Sciences and Tel-Aviv University was enabled thanks to COST Action MP1407 (e-MINDS).

Acknowledgments: The authors gratefully acknowledge the following persons: Remigiusz Kowalik for WDXRF measurements at AGH University of Science and Technology, Faculty of Non-Ferrous Metals, Krakow, Poland, Piotr Bobrowski for SEM observation and Łukasz Rogal for TEM observation at Institute of Metallurgy and Material Science, Polish Academy of Sciences, Krakow, Poland.

Conflicts of Interest: The authors declare no conflict of interest.

References

1. Eliaz, N.; Gileadi, E. *Physical Electrochemistry: Fundamentals, Techniques, and Applications*, 2nd ed.; Wiley-VCH: Weinheim, Germany, 2019.
2. Singh, V.B.; Singh, D.K. An overview on the preparation, characterization and properties of electrodeposited-metal matrix nanocomposites. *Nanosci. Technol.* **2014**, *1*, 1–20.
3. Kilic, F.; Gul, H.; Aslan, S.; Alp, A.; Akbulut, H. Effect of CTAB concentration in the electrolyte on the tribological properties of nanoparticle SiC reinforced Ni metal matrix composite (MMC) coating produced by electrodeposition. *Colloids Surf. A Physicochem. Eng. Asp.* **2013**, *419*, 53–60. [CrossRef]
4. Sajjadnejad, M.; Omidvar, H.; Javanbakht, M.; Pooladi, R.; Mozafari, A. Direct current electrodeposition of Zn and Zn-SiC nanocomposite coatings. *Trans. Inst. Mater. Finish.* **2014**, *92*, 227–232. [CrossRef]
5. Devaneyan, S.P.; Senthilvelan, T. Electro co-deposition and characterization of SiC in nickel metal matrix composite coatings on aluminium 7075. *Proc. Eng.* **2014**, *97*, 1496–1505. [CrossRef]
6. Walsh, F.C.; Ponce de Leon, C. A review of the electrodeposition of metal matrix composite coatings by inclusion of particles in a metal layer: An established and diversifying technology. *Trans. Inst. Met. Finish.* **2014**, *92*, 83–98. [CrossRef]

7. Kumar, M.K.P.; Venkatesha, T.V.; Pavithra, M.K. Development of Zn-SiC composite coatings: Electrochemical corrosion studies. *J. Electrochem. Sci. Eng.* **2015**, *5*, 25–36.
8. Singh, S.; Sribalaji, M.; Wasekar, N.P.; Joshi, S.; Sundararajan, G.; Singh, R.; Keshri, A.K. Microstructural, phase evolution and corrosion properties of silicon carbide reinforced pulse electrodeposited nickel-tungsten composite coatings. *Appl. Surf. Sci.* **2016**, *364*, 264–272. [CrossRef]
9. Wang, H.; Yao, S.; Matsumara, S. Electrochemical preparation and characterization of Ni/SiC gradient deposit. *J. Mater. Process. Technol.* **2004**, *145*, 299–302. [CrossRef]
10. Ger, M.D. Electrochemical deposition of nickel/SiC composites in the presence of surfactants. *Mater. Chem. Phys.* **2004**, *87*, 67–74. [CrossRef]
11. Lee, H.K.; Lee, H.Y.; Jeon, J.M. Codeposition of micro- and nano-sized SiC particles in the nickel matrix composite coatings obtained by electroplating. *Surf. Coat. Technol.* **2007**, *201*, 4711–4717. [CrossRef]
12. Gyftou, P.; Pavlatou, E.A.; Spyrellis, N. Effect of pulse electrodeposition parameters on the properties of Ni/nano-SiC composites. *Appl. Surf. Sci.* **2008**, *254*, 5910–5916. [CrossRef]
13. Dobosz, I.; Rudnik, E.; Burzynska, L. Codeposition of SiC particles with electrolytic nickel. *Arch. Metall. Mater.* **2011**, *56*, 665–670. [CrossRef]
14. Narasimman, P.; Pushpavanam, M.; Periasamy, V.M. Effect of Surfactant on the electrodeposition of Ni-SiC composites. *Port. Electrochim. Acta* **2012**, *30*. [CrossRef]
15. Muller, C.; Sarret, M.; Benballa, M. ZnNi/SiC composites obtained from an alkaline bath. *Surf. Coat. Technol.* **2002**, *162*, 49–53. [CrossRef]
16. Tulio, P.C.; Rodrigues, S.E.B.; Carlos, I.A. The influence of SiC and Al_2O_3 micrometric particles on the electrodeposition of ZnNi films and the ontainment of ZnNi-SiC and ZnNi-Al_2O_3 electrocomposite coatings from slightly acidic solutions. *Surf. Coat. Technol.* **2007**, *202*, 91–99. [CrossRef]
17. Tulio, P.C.; Carlos, I.A. Effects of SiC and Al_2O_3 particles on the electrodeposition of Zn, Co and ZnCo. I. Electrodeposition in the absence of SiC and Al_2O_3. *J. Appl. Electrochem.* **2009**, *39*, 283–291. [CrossRef]
18. Tulio, P.C.; Carlos, I.A. Effect of SiC and Al_2O_3 particles on the electrodeposition of Zn, Co and ZnCo: Electrodeposition in the presence of SiC and Al_2O_3 and production of ZnCo-SiC and ZnCo-Al_2O_3 coatings. *J. Appl. Electrochem.* **2009**, *39*, 1305–1311. [CrossRef]
19. Eliaz, N.; Gileadi, E. Induced codeposition of alloys of tungsten, molybdenum and rhenium with transition metals. In *Modern Aspects of Electrochemistry*; Vayenas, C.G., White, R.E., Gamboa-Aldeco, M.E., Eds.; Springer: New York, NY, USA, 2008; Volume 42, p. 191.
20. Rosen, B.A.; Gileadi, E.; Eliaz, N. Microstructure and composition of pulse plated Re–Ni alloys on a rotating cylinder electrode. *J. Electroanal. Chem.* **2014**, *731*, 93–99. [CrossRef]
21. Nusbaum, T.; Rosen, B.A.; Gileadi, E.; Eliaz, N. Effect of pulse on-time and peak current density on pulse plated Re-Ni alloys. *J. Electrochem. Soc.* **2015**, *162*, D250–D255. [CrossRef]
22. Fustes, J.; Gomes, A.; da Silva Pereira, M.I. Electrodeposition of Zn-TiO_2 nanocomposite fils-effect of bath composition. *J. Solid State Electrochem.* **2008**, *12*, 1435–1443. [CrossRef]
23. Nemes, P.I.; Lekka, M.; Fedrizzi, L.; Muresan, L.M. Influence of the electrodeposition current regime on the corrosion resistance of Zn–CeO_2 nanocomposite coatings. *Surf. Coat. Technol.* **2014**, *252*, 102–107. [CrossRef]
24. Frade, T.; Bouzon, V.; Gomes, A.; da Silva Pereira, M.I. Pulsed-reverse current electrodeposition of Zn and Zn-TiO_2 nanocomposite films. *Surf. Coat. Technol.* **2010**, *204*, 3592–3598. [CrossRef]
25. Gomes, A.; da Silva Pereira, M.I. Pulsed electrodeposition of Zn in the presence of surfactants. *Electrochim. Acta* **2006**, *51*, 1342–1350. [CrossRef]
26. Roventi, G.; Belezze, T.; Fratesi, R. Rivestimenti compositi Zn-SiC ottenuti per elettrodeposizione. Proceedings of XI AIMAT National Congress, Gaeta, Italy, 16–19 September 2012; pp. 459–462.
27. Roventi, G.; Belleze, T.; Fratesi, R. Electrodeposition of Zn-SiC nanocoposite coatings. *J. Appl. Electrochem.* **2013**, *43*, 839–846. [CrossRef]
28. Sajjadnejad, M.; Mozafari, A.; Omidvar, H.; Javanbakht, M. Preparation and corrosion resistance of pulse electrodeposited Zn and Zn-SiC nanocomposite coatings. *Appl. Surf. Sci.* **2014**, *300*, 1–7. [CrossRef]
29. Conway, B.E. *Modern Aspects of Electrochemistry*; Springer: New York, NY, USA, 2005; Volume 38.
30. Cornelsen, P.A.; Quintanilha, R.C.; Vidotti, M.; Gorin, P.A.J.; Simas-Tosin, F.F.; Riegel-Vidotti, I.C. Native and structurally modified gum arabic: Exploring the effect of the gum's microstructure in obtaining electroactive nanoparticles. *Carbohydr. Polym.* **2015**, *119*, 35–43. [CrossRef] [PubMed]

31. Afifi, S.E.; Ebaid, A.R.; Hegazy, M.M.; Barakat, A.K. The effect of additives on Zinc deposited from Zinc sulfate solutions. *J. Miner. Met. Mater. Soc.* **1992**, *44*, 32–34. [CrossRef]
32. Recendiz, A.; Gonzalez, I.; Nava, J.L. Current efficiency studies of the zinc electrowinning process on aluminum rotating cylinder electrode (RCE) in sulfuric acid medium: Influence of different additives. *Electrochim. Acta* **2007**, *52*, 6880–6887. [CrossRef]
33. Zhang, H.; Shan, G.; Liu, H.; Xing, J. Surface modification of γ-Al_2O_3 nano-particles with gum arabic and its applications in adsorption and biodesulfurization. *Surf. Coat. Technol.* **2007**, *201*, 6917–6921. [CrossRef]
34. Chu, H.; Zhang, J.; An, M. Influences of SiC concentration on Sn/SiC nanocomposite electrodeposition. *Int. J. Electrochem. Sci.* **2013**, *8*, 1871–1884.
35. Inam, F.; Heaton, A.; Brown, P.; Pijs, T.; Reece, M.J. Effects of dispersion surfactants on the properties of ceramic-carbon nanotube (CNT) nanocomposites. *Ceram. Int.* **2014**, *40*, 511–516. [CrossRef]
36. Wu, W.; Eliaz, N.; Gileadi, E. Electrodeposition of Re-Ni alloys from aqueous solutions with organic additives. *Thin Solid Films* **2016**, *616*, 828–837. [CrossRef]
37. Eliaz, N.; Venkatakrishna, K.; Hegde, A.C. Electroplating and characterization of Zn–Ni, Zn–Co and Zn–Ni–Co alloys. *Surf. Coat. Technol.* **2010**, *205*, 1969–1978. [CrossRef]
38. Hegde, A.C.; Venkatakrishna, K.; Eliaz, N. Electrodeposition of Zn–Ni, Zn–Fe and Zn–Ni–Fe alloys. *Surf. Coat. Technol.* **2010**, *205*, 2031–2041. [CrossRef]
39. Thangaraj, V.; Eliaz, N.; Hegde, A.C. Corrosion behavior of composition modulated multilayer Zn–Co electrodeposits produced using a single-bath technique. *J. Appl. Electrochem.* **2009**, *39*, 339–345. [CrossRef]
40. Eliaz, N.; Sridhar, T.M.; Gileadi, E. Synthesis and characterization of nickel tungsten alloys by electrodeposition. *Electrochim. Acta* **2005**, *50*, 2893–2904. [CrossRef]
41. Samal, S.K.; Dash, M.; Van Vlierberghe, S.; Kaplan, D.L.; Chiellini, E.; van Blitterswijk, C.; Moroni, L.; Dubruel, P. Cationic polymers and their therapeutic potential. *Chem. Soc. Rev.* **2012**, *41*, 7147–7194. [CrossRef] [PubMed]
42. Sahoo, N.; Sahoo, R.K.; Biswas, N.; Guha, A.; Kuotsu, K. Recent advancement of gelatin nanoparticles in drug and vaccine delivery. *Int. J. Biol. Macromol.* **2015**, *81*, 317–331. [CrossRef] [PubMed]
43. Chang, Y.; Hu, Y.; McClement, D.J. Competitive adsorption and displacement of anionic polysaccharides (fucoidan and gum arabic) on the surface of protein-coated lipid droplets. *Food Hydrocoll.* **2016**, *52*, 820–826. [CrossRef]
44. Masuelli, M.A. Hydrodynamic properties of whole arabic gum. *Am. J. Food Sci. Technol.* **2013**, *1*, 60–66.
45. Méndez, A.; Moron, L.E.; Ortega-Borges, R.; Meas, Y.; Trejo, G. EQCM study of the adsorption of polyethyleneglycol with different molecular weights and its coadsorption with Cl^- ions on Pt in perchloric acid solution. *Int. J. Electrochem. Sci.* **2010**, *5*, 1754–1772.
46. Mendez, A.; Moron, L.E.; Ortiz-Frade, L.; Meas, Y.; Ortega-Borges, R.; Trejo, G. Thermodynamic studies of PEG (Mw 20,000) adsorption onto a polycrystalline gold electrode. *J. Electrochem. Soc.* **2011**, *158*, F45–F51. [CrossRef]
47. Mendez, A.; Meas, Y.; Ortega-Borges, R.; Trejo, G. Thermodynamic study of PEG (Mw 20,000) adsorption in the presence of Cl-anions onto a polycrystalline gold electrode. *J. Electrochem. Soc.* **2012**, *159*, F48. [CrossRef]
48. Banik, S.J.; Akolkar, R. Suppressing dendrite growth during zinc electrodeposition by PEG-200 additive. *J. Electrochem. Soc.* **2013**, *160*, D519–D523. [CrossRef]
49. Ballesteros, J.C.; Diaz-Arista, P.; Meas, Y.; Ortega, R.; Trejo, G. Zinc electrodeposition in the presence of polyethylene glycol 20,000. *Electrochim. Acta* **2007**, *52*, 3686–3696. [CrossRef]
50. Gomes, A.; da Silva Pereira, M.I. Zn electrodeposition in the presence of surfactants Part I. Voltammetric and structural studies. *Electrochim. Acta* **2006**, *52*, 863–871. [CrossRef]
51. Chen, Y.C.; Kuo, S.L.; Lee, J.L.; Ke, S.T.; Wong, C.H.; Ger, M.D. The influence of surfactant CTAB on the microstructure and material properties of Nickel microelectroforming. *Key Eng. Mater.* **2008**, *364*, 346–350.
52. Tripathy, B.C.; Das, S.C.; Hefter, G.T.; Singh, P. Zinc electrowinning from acidic sulfate solutions: Part I: Effect of sodium lauryl sulfate. *J. Appl. Electrochem.* **1997**, *27*, 673–678. [CrossRef]
53. Kazimierczak, H.; Szymkiewicz, K.; Rogal, Ł.; Gileadi, E.; Eliaz, N. Direct current electrodeposition of Zn-SiC nanocomposite coatings from citrate bath. *J. Electrochem. Soc.* **2018**, *165*, D526–D535. [CrossRef]
54. Kazimierczak, H.; Szymkiewicz, K.; Bobrowski, P.; Świątek, Z.; Rogal, Ł.; Gileadi, E.; Eliaz, N. The effect of SiC nanoparticle size on the electrodeposition of Zn–SiC nanocomposite coatings from citrate bath. *J. Electrochem. Soc.* **2018**, *165*, D774–D782. [CrossRef]

55. Pushpavanam, M.; Balakrishnan, K. Zinc-Nickel alloy deposition in the presence of citrate ions. *J. Appl. Electrochem.* **1996**, *26*, 1065–1069. [CrossRef]
56. Kazimierczak, H.; Ozga, P.; Jalowiec, A.; Kowalik, R. Tin–Zinc alloy electrodeposition from aqueous citrate baths. *Surf. Coat. Technol.* **2014**, *240*, 311–319. [CrossRef]
57. Kazimierczak, H.; Ozga, P. Electrodeposition of Sn–Zn and Sn–Zn–Mo layers from citrate solutions. *Surf. Sci.* **2013**, *607*, 33–38. [CrossRef]
58. Kazimierczak, H.; Ozga, P.; Socha, R.P. Investigation of electrochemical co-deposition of zinc and molybdenum from citrate solutions. *Electrochim. Acta* **2013**, *104*, 378–390. [CrossRef]
59. Kazimierczak, H.; Hara, A.; Bigos, A.; Ozga, P. Electrodeposition of Zn-Mn-Mo layers from citrate-based aqueous. *Electrochim. Acta* **2016**, *202*, 110–121.
60. Pereira, M.S. The influence of sorbitol on zinc film deposition, zinc dissolution process and morphology of deposits obtained from alkaline bath. *J. Appl. Electrochem.* **2006**, *36*, 727–732. [CrossRef]
61. Hsieh, J.C.; Hu, C.C.; Lee, T.C. The synergistic effects of additives on improving the electroplating of Zinc under high current densities. *J. Electrochem. Soc.* **2008**, *155*, D675–D681. [CrossRef]